Robotic Scanning Device for Intraoperative Thyroid Gland Endomicroscopy

HAIBO WANG, SHUXIN WANG, JINHUA LI, and SIYANG ZUO

The Key Laboratory of Mechanism Theory and Equipment Design of Ministry of Education, Tianjin University, Tianjin 300072, China

Associate Editor Xiaoxiang Zheng oversaw the review of this article.

Abstract—Probe-based confocal laser endomicroscopy has a high potential to be a promising tool that can provide intraoperative high-resolution *in vivo* morphological imaging at cellular and subcellular levels for thyroidectomy, and allow real-time assessment of tumor margins. However, the typical images acquired with this technique cover a very small area limited by the field of view of the probe, accompanied by tissue deformation and inconsistent probe–tissue contact when operated manually. In this paper, a novel compact robotic device for large area scanning has been developed. The device can scan a large surface in a spiral trajectory by rotating the tip frame along the spiral groove of the base frame. The fiber Bragg grating sensor with a passive linear structure is used to detect and maintain a stable probe–tissue contact force during scanning. An active linear actuation is also integrated for adjusting the probe–tissue contact level prior to each scan. Results demonstrate that the scanning device ensures a suitable probe–tissue contact force and compensates for simulated hand tremor. Mosaicing results of lens tissue paper and porcine belly tissue with both bench and hand-held experiments show the effectiveness and usability of the device, demonstrating the potential clinical value of the system.

Keywords—Thyroidectomy, Confocal endomicroscopy, Force sensing, Image mosaicing, Mechanical design.

INTRODUCTION

Over the last few decades, thyroid cancer incidence has been appreciably increasing in most areas of the world. It was estimated that there were 230,000 cases of thyroid cancer among women and 70,000 among men, and numbers of deaths from thyroid cancer were 27,000 in women and 13,000 in men in 2012.[39] The most effective treatment for thyroid cancer invading the larynx and trachea is a complete surgical resection of the tumor. Surgical options in this situation include the shave procedure, partial laryngectomy, and total laryngectomy.[10] However, complete tumor removal is currently confirmed post-operatively by tissue biopsy through histology. In some cases, when a patient is receiving surgery in an operating room, the surgeon has to wait for the results of the pathology analysis in order to orient the procedure Current extemporaneous tissue biopsy requires at least 20 min for this process.[12] If there still exist some cancer cells on the edges of excised tissues, the patient will be required to return to the operating theatre for further surgery.[35] The re-operation has many shortcomings, such as the risk of infections, poor cosmesis, long-term hospitalization and higher costs.[19]

In recent years, the technology that could provide *in situ*, , *in vivo* functional imaging of the target organs at cellular and subcellular levels has become an important research topic. The aim of this technology is to perform intraoperative optical biopsies on the target to determine whether cancer patients are appropriate candidates for surgery or would be better suited to chemotherapy or radiation treatment. The core technology of optical biopsy is confocal endomicroscopy,[17] which has the technical advantages and physical properties to provide high resolution, real-time, and *in situ* imaging at cellular and subcellular levels.[5,26–28] It has the potential to strengthen diagnosis and provide valuable real-time tissue information during minimally invasive surgery, and to avoid the risk of tissue damage from standard tissue biopsy. Fluorescence confocal endoscope has been developed for imaging and diagnosing carcinoma *in situ*, such as in the gastrointestinal tract lumen,[25,41] lung,[29] and peritoneal cavity.[33] In

---

Address correspondence to Siyang Zuo, The Key Laboratory of Mechanism Theory and Equipment Design of Ministry of Education, Tianjin University, Tianjin 300072, China. Electronic mail: siyang_zuo@tju.edu.cn

particular, some studies have demonstrated that the confocal endomicroscopy is a useful method for parathyroid glands and neck dissection.[6,7]

However, the field-of-view of endomicroscopy is limited in observation range (typically smaller than 0.5 mm in diameter for high resolution probe), and only partial characters could be studied from the images. Thus, a micro panoramic image of the target is necessary for the surgeon to make the right decision. Mosaicing algorithms could solve this problem by merging the adjacent images together to display large field-of-view image.[23,36] The functional status of the target could be fully demonstrated to the surgeon from the mosaicing results.

Though fair quality mosaicings can be obtained by manually moving the probe across the tissue surface, the quality of the images is affected by many factors such as the image features, the velocity of probe, the probe–tissue contact state and the scanning trajectory. Thus, controlling the probe to obtain consistent and stable images is necessary for endomicroscopy to be widely used in modern clinical practice.[43] Several groups have presented a few compact miniaturized mechatronic devices to facilitate smooth and consistent movement of the probe on the tissue surface.[9,11,31,33,40,42] For example, Rosa *et al.* developed a scanning device using hydraulic micro-balloons for the organs inside the abdominal cavity.[33] Erden *et al.* proposed a distal scanner using the conic-spiral mechanism to perform automated spiral scan with the probe.[11] Zuo *et al.* developed a balloon linkage scanning mechanism[40] for microscopic imaging during breast conserving surgery.

For the devices described in Refs. 11 and 33 the areas imaged by these designs are typically less than 3 mm^2. The requirements for scanning the cavity in thyroidectomy are somewhat different. The actual size of the thyroid tumor can range between 0.1 and 6 cm.[18] Thus, a large surface needs to be scanned over during thyroidectomy. So far, several studies have shown large area mosaicings using miniature mechanized scanning of endomicroscope probes[9,40,42] However, all of these devices[9,11,31,33,40,42] are lack of force sensing and active linear actuation for adjusting tissue contacts. Indeed, the fluctuation of the contact force has an important influence on the clarity of the images. This application therefore requires a new robotic device which is capable of scanning over a large area of tissue with force sensing and stable tissue contacts, but with simpler mechanical design.

Force sensing based on fiber Bragg grating (FBG) sensors is a promising approach to measure the force of medical instruments. FBG sensor offers a number of advantages over the strain gage, including lightweight structures, the absence of electromagnetic interference,

high sensitivity, good repeatability, fast response, and a potentially low cost. Due to these special advantages of the FBG sensor, it has found several applications in a broad range of disciplines such as aerospace, medicine and civil engineering, where they can be used as force gauges, shape and temperature sensors. For endomicroscopy imaging, the probe–tissue contact force plays a more important role in obtaining good quality images than other factors. Thus, we applied FBG sensors to sense the force between the instrument tip and soft tissues. For force sensing, Russo *et al.* used FBG sensors in laser assisted transurethral surgery to sense contact forces.[34] A three-axis FBG force sensor was investigated by Guo *et al.* for robot finger.[14] Other applications for force sensing include a contact force sensing in eye surgery[2,15] and tool-to-tissue interaction force sensing in a hand-held micromanipulator.[13]

In this paper, we propose a new endomicroscopy scanning device to perform optical biopsies on the target surface in a spiral trajectory with stable probe–tissue contact during the neck dissection or thyroidectomy (Fig. 1). The FBG sensor monitors the contact force between the probe and tissue. With the motion of the device, the probe performs a specific spiral scanning trajectory. Mosaicing algorithms process the experimental images, obtaining a large scale view of the target. Experimental results demonstrate that the device can achieve large area endomicroscopy mosaicing during both bench and hand-held scanning.

MATERIALS AND METHODS

Scanning Mechanism

As the endomicroscopy image is affected by many factors as mentioned above, to obtain high-quality mosaicing images, the probe needs to make stable and consistent contact with the target tissue during scanning. We chose spiral trajectory as an effective way to scan cover the target tissue surface. A primary advantage of the spiral trajectory is no mutation in the direction of velocity compared with other trajectories. If there is any mutation in the direction of velocity, the frame rate of imaging system may not be fast enough to follow the sudden rise of the velocity of the probe. Hence, the mutations in scanning direction can also lead to large tissue deformation, which could affect the efficiency of the scanning and mosaicing. Figure 2 illustrates the scanning mechanism. The scanning unit consists of the tip frame, tip slider, slider fixture, base slider, rotation gear, bearing and base frame. The Nitinol lever (0.35 mm in diameter) of the tip frame is inserted into and guided by the spiral groove (0.4 mm
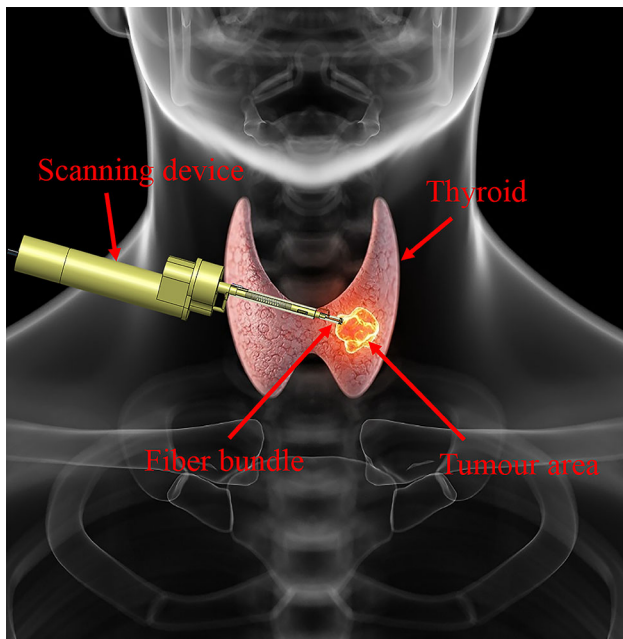
FIGURE 1. Concept of the system during thyroidectomy.

in width) of the base frame. The spiral groove is fabricated in the base frame by high precision wire-cut EDM (with a tolerance of $\pm$ 0.005 mm). The tip frame is also guided by a linear groove on the slider fixture. The slider fixture is sandwiched between the tip slider and base slider, which can guide the tip frame to achieve a stable spiral trajectory and prevent unexpected motion. The rotation gear and base frame are fixed to the bearing structure to achieve separated rotating motion. Thus, if the slider fixture is rotated, the tip frame will rotate along the spiral groove of the base frame, and then achieve a spiral trajectory. Since the field-of-view captured by the endomicroscopy system is 0.8 mm in diameter in this study, the spiral loop spacing is designed to be 0.8 mm, which could make edges of the scanning images just touch. The gear fixture is driven by a pair of rotation gears though a high-resolution brushless DC-servomotor equipped with a gear head and a Hall effect sensor (1226E 012 B K1885 Faulahaber SA, Germany), which can achieve an accurate closed-loop position control and enough torque output for scanning soft tissue.

An active linear actuation has been integrated into the device to adjust the contact between the probe and tissue. The principle of the mechanism is demonstrated in Fig. 3a. An M3 screw is connected with the DC-servomotor by coupling, while the nut is inserted into the slide block. The slide block could slide smoothly along the linear guide, which drives the scanning tip to achieve a linear motion. Then, tissue contacts could be adjusted by this mechanism.

The imaging fiber bundle is fixed to the distal module by set screws. The distal module is connected with the tip frame by a rotation-preventing mechanism as shown in Fig. 3b. Two rotation bearings are fixed to the proximal module with embedded steel balls which rotate during scanning. Combined with an elastic rubber band, this structure prevents the endomicroscope probe from rotating around its axis during scanning.

A FBG sensor is cast in a spring by Silica Gel, which is used as a force sensor to detect probe–tissue contact level during the scanning. The spring structure can also ensure consistent contact between the distal end and tissue. The FBG sensing unit is installed into the middle module and connects with the distal module. When the probe compresses the tissue, the wavelength of the reflected wave of the FBG sensor will be changed, reflecting the contact force between the probe and tissue. This structure is designed to achieve a suitable probe–tissue contact force and compensate for hand tremor with force sensing.

The scanning prototype is illustrated in Fig. 3c. The scanning shaft is 9 mm in maximum outer diameter and 118 mm in length. The structure is fabricated in ABSplus. A cylindrical cover with 29 mm in diameter encloses the actuation unit. The total length of the scanning device is 288 mm, and the total weight of the scanning prototype is 255 g, thus making it suitable for using as a hand-held device. The scanning shaft can be easily separated from the actuation unit, thus being helpful for cleaning and sterilization. Hence, the modules can also be separated, making it possible to be used in a patient-specific design process.

Kinematics, Control Algorithm and Trajectory

A user software has been developed in Labview (National Instruments). The device can be controlled by entering different motion parameters. The total system consists of the motion control and force sensing unit, the scanning device and the endomicroscopy system, allowing combination of scanning control, force sensing and image acquisition for real-time use (Fig. 4).

A compact and continuous mosaicing could be achieved by scanning the tissue in a spiral trajectory with the probe. The tangential velocity $v_{\text{tangential}}$ and the loop spacing Δh are two important parameters of the scanning. The tangential velocity is closely related to the radius R and angular velocity of the motor, which can be expressed as:

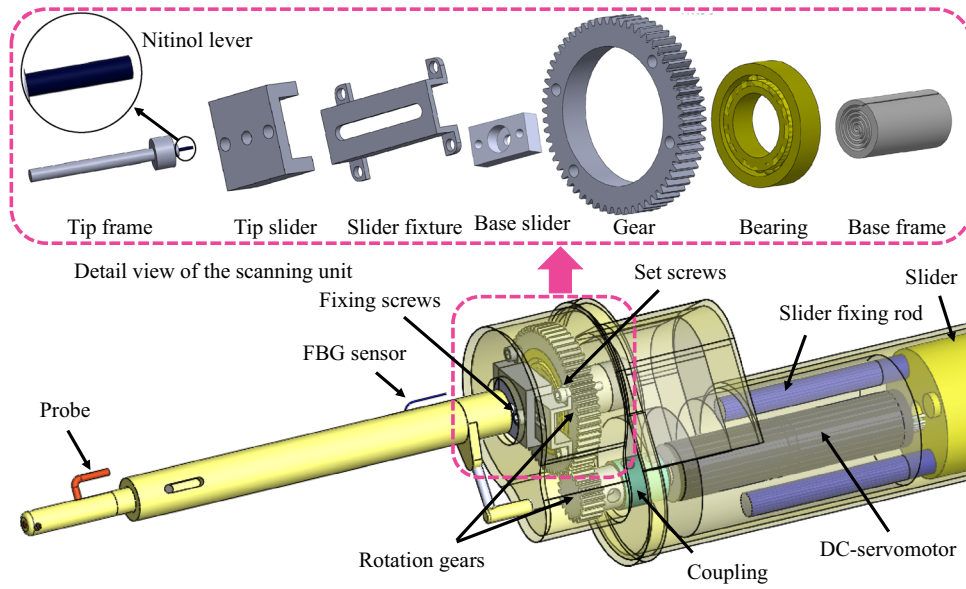$$v_{\text{tangential}} = \frac{W_{m1} \cdot 2\pi \cdot R}{\mu_1 \cdot 60} \ (\text{mm/s}) \qquad (1)$$

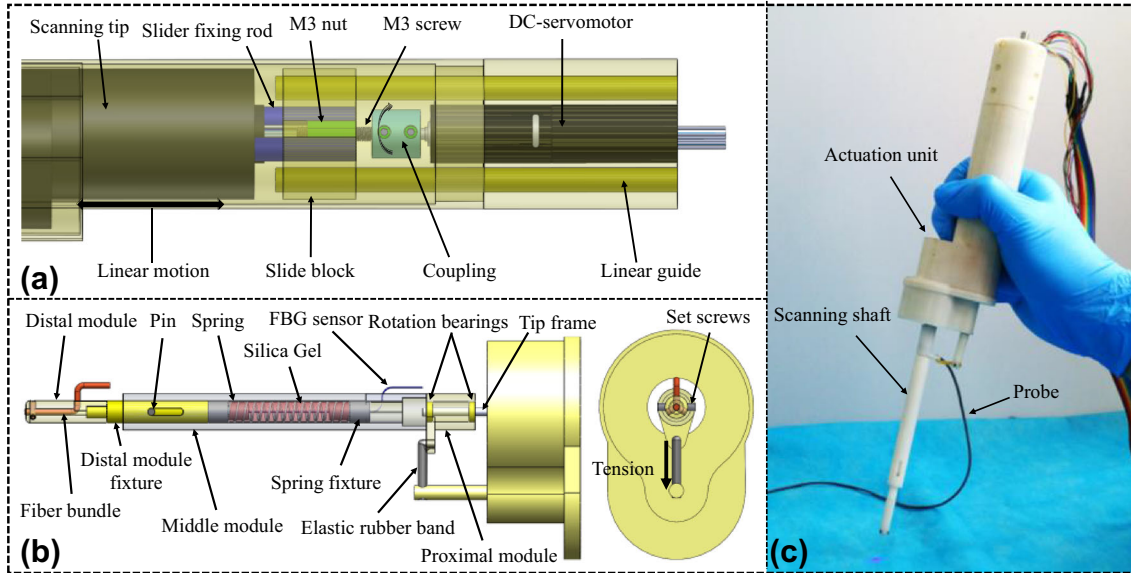**FIGURE 2. The configuration and detail view of the scanning mechanism.**

FIGURE 3. The prototype of the scanning device, showing (a) the configuration of the linear actuation; (b) the configuration of the scanning tip; (c) the image of the scanning device.

$$R = \Delta h \cdot \frac{W_{m1} \cdot t}{\mu_1 \cdot 60} \ (\text{mm}) \qquad (2)$$

where μ_1 is the gear reduction ratio of the scanning mechanism, W_{m1} is the angular velocity of DC-servomotor, and R is the radius of the spiral trajectory. Δh (0.8 mm) is a constant value determined by the groove on the base frame.

The theoretical mosaicing area S_{spiral} achieved by the spiral trajectory is related to the angular velocity W_{m1} and the loop spacing Δh. It can be expressed as follows:

When,

$$\frac{W_{m1} \cdot t}{\mu_1 \cdot 60} \leq 1$$

$$S_{\text{spiral}} = \int_0^t \frac{R^2}{2} \, \mathrm{d}\alpha = \int_0^t \frac{\pi \cdot \Delta h^2 \cdot W_{m1}^3 \cdot t^2}{\mu_1^3 \cdot 60^3} \, \mathrm{d}t \ (\text{mm}^2) \quad (3)$$

When,

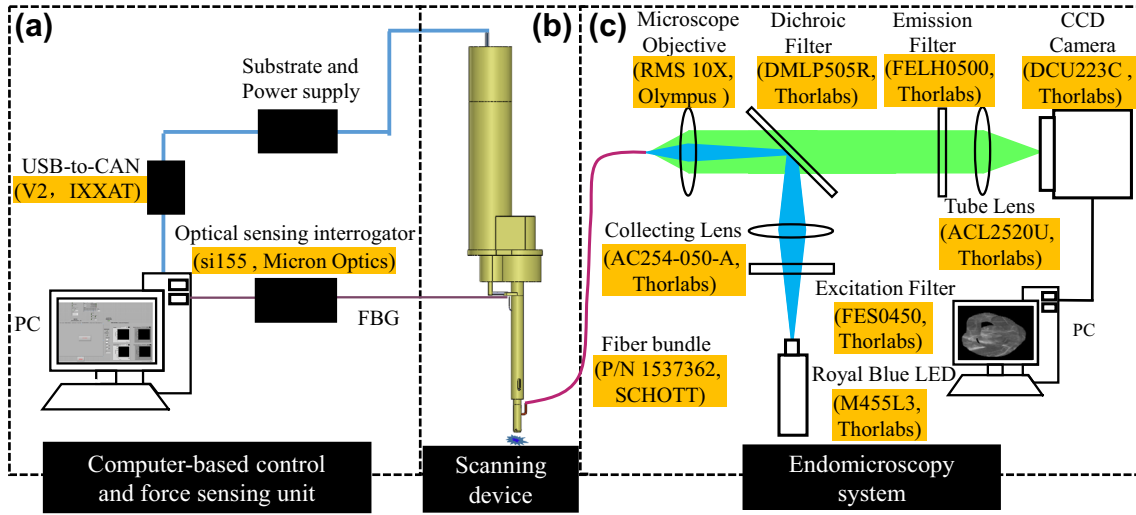$$\frac{W_{m1} \cdot t}{\mu_1 \cdot 60} \geq 1$$

FIGURE 4. The system configuration of scanning device, showing (a) the computer based control and force sensing unit; (b) the robotic scanning device; (c) the endomicroscopy system.

$$S_{\text{spiral}} = \int_{t_1}^{t} \frac{R^2}{2} d\alpha = \int_{t-\frac{\mu_1 \cdot 60}{W_{m1}}}^{t} \frac{\pi \cdot \Delta h^2 \cdot W_{m1}^3 \cdot t^2}{\mu_1^3 \cdot 60^3} dt \ (\text{mm}^2)$$

(4)

Combining (3) and (4), the complete expression for the theoretically covered mosaicing area S_{spiral} can be given by (5).

$$S_{\text{spiral}} = \begin{cases} \int_{0}^{t} \frac{\pi \cdot \Delta h^2 \cdot W_{m1}^3 \cdot t^2}{\mu_1^3 \cdot 60^3} dt \ (\text{mm}^2) & \frac{W_{m1} \cdot t}{\mu_1 \cdot 60} \leq 1 \\ \int_{t-\frac{\mu_1 \cdot 60}{W_{m1}}}^{t} \frac{\pi \cdot \Delta h^2 \cdot W_{m1}^3 \cdot t^2}{\mu_1^3 \cdot 60^3} dt \ (\text{mm}^2) & \frac{W_{m1} \cdot t}{\mu_1 \cdot 60} \geq 1 \end{cases}$$

(5)

For linear actuation, the velocity v_{axial} and length l_{axial} of the linear motion are related to the angular velocity and the pitch of the thread used for driving. The relationship can be expressed as follows:

$$v_{\text{axial}} = \frac{W_{m2}}{\mu_2 \cdot 60} \cdot P \ (\text{mm/s})$$

(6)

$$l_{\text{axial}} = v_{\text{axial}} \cdot t \ (\text{mm})$$

(7)

where μ_2 is the gear reduction ratio of gearbox, W_{m2} is the angular velocity of DC-servomotor, and $P(0.5 \text{ mm})$ is a constant value determined by the thread (M3) used in the device.

The relationship between mosaicing area and time with different angular velocities of motor is shown in Fig. 5. Note that the probe used in this system has the ability to observe an area of 0.8 mm in diameter, so that the loop spacing of spiral trajectory is set at 0.8 mm. Theoretically, it could achieve a mosaicing without gap.

Force Sensing

The force sensing system is illustrated in Fig. 4a. By sending the broadband light into the FBG optic fiber, the Bragg grating parts reflect one type of center wavelength peak (1550 nm in this study). By sensing the reflected wavelength λ_B, the strain of the Bragg grating can be calculated.

$$\lambda_B = 2 \cdot n_{eff} \cdot \Lambda \ (\text{nm})$$

(8)

where λ_B and Λ are the effective refractive index and the length of the grating period, respectively.[16] The used FBG node is 10 mm in length and 160 μm in diameter. An optical sensing interrogator, si155 from Micron Optics Inc. (four channels, with resolution of 0.001 nm and scan frequency of 100 Hz) is used to monitor the wavelength variation of FBG sensor. Since the probe needs to contact with the tissue for obtaining images during scanning, changes in probe–tissue contact force result in the wavelength variation. The relationship between wavelength variation and contact force could be established by a series of calibration experiments.

Visualization and Mosaicing

The endomicroscopy system used in this study is an in-house low cost laser scanning system. The imaging fiber bundle used in this system is a composition of 18,000 cores, and each could provide a 'pixel' on the image captured. It has a length of 895 mm and a diameter of 1.27 mm. A field-of-view of 900 μm image is captured. The main features of the fiber bundle are the outstanding performance of flexibility and large field of view, which meet the requirements of the robotic scanning device.
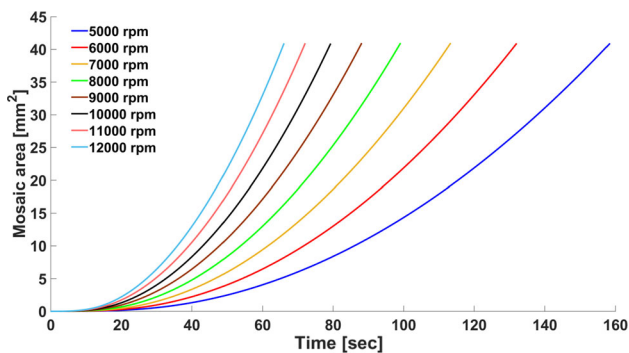
FIGURE 5. The relationship between mosaicing area and time with different angular velocities of motor.

The optical system connected with the scanning device is demonstrated in Fig. 4c. The optical system is established based on previously reported system for *in situ* cellular imaging.[24] The schematic of the optical system can be illustrated as follows. The targeted tissue has been previously stained using a fluorescent agent such as fluorescein or acriflavine. A 450 nm blue LED was used as the illumination source. The light passed through the low-pass excitation filter with a cutoff wavelength of 450 nm, and focused on the dichroic filter by a collecting lens. The reflected beam from the dichroic filter focused on the imaging fiber bundle by a microscope objective. Then the fluorescent of stained tissue was relayed by the probe and transmitted by the dichroic filter, a tube lens and an emission filter whose cutoff wavelength was 500 nm. The fluorescent emission was finally imaged onto a CCD camera. Images are acquired at 15 fps by the system and a computer connected with the CCD camera could record and store the image information.

The algorithms used to process the video were similar to the algorithms previously demonstrated in detail.[1,3,4] For mosaicing, a cross-correlation based mosaicing algorithm was developed in Matlab. The normalized two dimensional cross-correlation was computed from a template extracted from each image and the previous image. The position of the peak of the cross-correlation was considered to be the correct shift between the two images. To create robust mosaicing, each image was inserted into the mosaicing with the correct shift corresponding to the previous image using distance-weighted alpha blending to smooth the transition between frames, over-writing any existing pixel values.

RESULTS

Mechanical Performance Evaluation

In order to evaluate the scanning trajectory of the device, an NDI Aurora electromagnetic tracking sys-

tem (NDI Corp., USA) was used as shown in Fig. 6a. A mini electromagnetic sensor with 6 DOFs was inserted and fixed into the channel of distal module. The robotic scanning device was fixed on the workbench and perpendicular to the field generator. Then we performed the spiral scans four times. We chose one set of dates randomly to evaluate the workspace and trajectory. The results are shown in Figs. 6b–6f. The 3D trajectory of spiral scanning with linear motion is illustrated in Fig. 6b. Figures 6d–6f show the target and actual *x*, *y* and *z* positions, while the 2D spiral trajectory is shown in Fig. 6c.

Force Sensing Validation

To validate the relationship between the force and wavelength variation, a bench experiment with the robotic device and dynamometer was performed (Fig. 7a). To minimize the temperature sensitivity in the force sensing process, all the following experiments were tested at a stable room temperature (26 °C). The constant room temperature was achieved by an air conditioner and measured by a temperature meter. The experiments were performed after the stable temperature was confirmed. The scanning tip was controlled by active linear actuation to contact with the dynamometer perpendicularly with different contact forces. Then, the dynamometer with resolution of 0.01 N recorded the contact force and the interrogator recorded the center wavelengths of the FBG sensor. The calibration results between the wavelength variation and contact force are illustrated in Fig. 7b. We have tested 3 different materials (metal, silica gel and porcine belly tissue) that have different stiffness for force calibration. The relationship between force and wavelength variation has shown a nonlinear manner. This is due to nonlinear hyperelastic law of the spring structure.

In case of using the prototype as a hand-held device, the probe–tissue contact force is closely related with physiological motion of the hand. The frequency and typical amplitude of the hand tremor are 8–12 Hz and 50 μm p–p respectively.[8] Furthermore, the endomicroscopy probe can obtain stable images when the contact force is between 0.1 and 0.5 N.[20,30]

To confirm the ability of the device to keep consistent probe–tissue contact, we performed bench experiments with a linear DC-servomotor to simulate the hand tremor in axis direction as shown in Fig. 7c. The tip of linear motor shaft was lined with the tissue paper stained with acriflavine to allow imaging. The linear motor was controlled to provide linear motion with a p–p amplitude of 100 μm and frequency of 8 Hz.

Images captured at trough, centre and crest of the tremor without the passive linear structure are shown
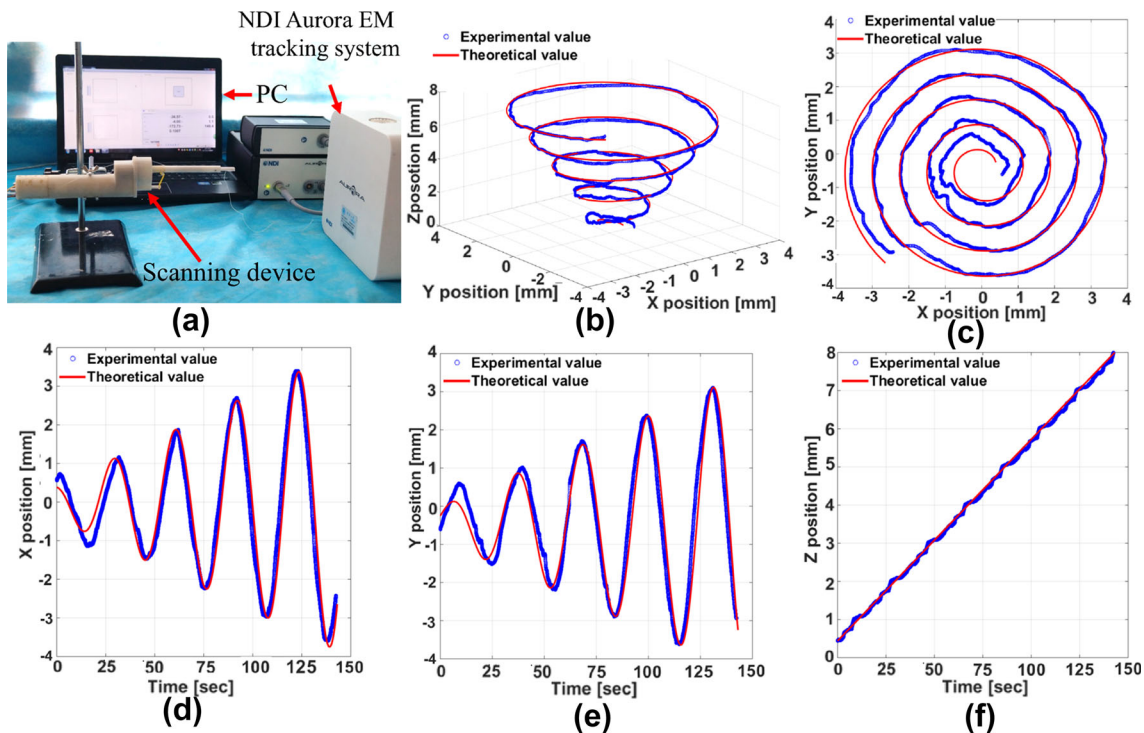
FIGURE 6. Mechanical performance of the scanning device, showing (a) the experiment setup for verifying mechanical performance of the scanning device; (b) 3D trajectory of spiral scanning with linear motion; (c) 2D spiral trajectory; (d) X position; (e) Y position; (f) Z position.

in Fig. 7e. On the other hand, Fig. 7f shows images captured with the passive linear structure. The force variation is shown in Fig. 7d. The fibrous structures of lens tissue paper can be clearly distinguished during the whole experiment with the passive linear structure in Fig. 7f. However, without the passive linear structure, the images of tough and centre parts of the tremor (Fig. 7e) are not clear enough. The image of crest part of the tremor in Fig. 7e shows a moment of fair quality image. That is because the probe tended to push out tissue paper in that moment. This large contact force could drag the tissue and affect the mosaicing results. To achieve smooth tissue scanning motion with small tissue deformation, a suitable force (ideally smaller than 0.5 N) is important. During the experiments with passive linear structure, the contact force variation was approximately between 0.11 and 0.44 N (Fig. 7d), which means the passive linear structure was sufficiently good for obtaining good-quality imaging in a hand tremor situation.

Bench Experiment

We confirmed the ability of the device to obtain consistent mosaicing for bench experiments with lens tissue paper (Fig. 8a). The scanning device was fixed on a passive arm. Firstly, the scanning tip was controlled by the active linear actuation to achieve an appropriate probe–tissue contact. Then, we performed the spiral scanning. During the scanning, the endomicroscopy system captured the images of the lens tissue paper and the optical sensing interrogator recorded the wavelength of FBG sensor. We performed the spiral scans four times and chose a quite satisfactory mosaicing without gap (Fig. 8b) and a mosaicing with a gap at the center (Fig. 8c). Figures 8b and 8c illustrate the mosaicing results from the spiral scanning which covered an area of 17.87 and 18.98 mm^2 respectively, while the intended automatic scanning areas were 21.4 and 24.79 mm^2 respectively. Thus the ratios of the covered area to the intended areas are 0.84 and 0.77 respectively. A large number of fibrous tissues can be clearly observed from the mosaicings. There are small gaps between the loops of the spiral (Fig. 8b). The cause of the gaps is likely to be the combination of mosaicing errors, positioning errors and deformation of the scanned surface.

Figure 8d shows the force variation (between 0.19 and 0.38 N) during bench experiments with lens tissue paper. That is a suitable range of contact force for obtaining stable images during the scanning.

Hand-Held Experiment

The above results of bench experiments demonstrate the capability of the system to achieve mosaicing with
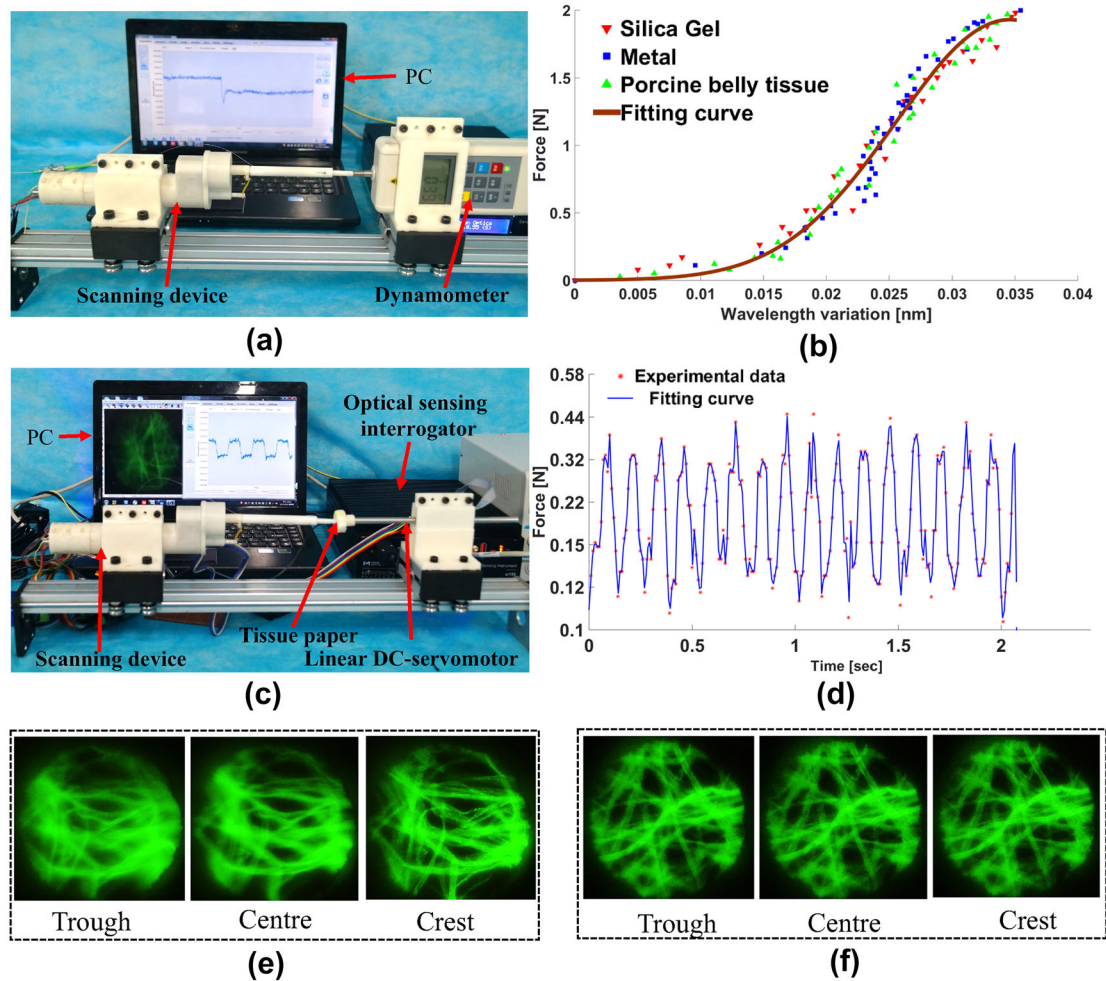
FIGURE 7. Force sensing performance of the scanning device, showing (a) the experiment setup for calibration; (b) the calibration results between the wavelength variation and contact force; (c) the experiment setup for bench experiment to verify probe–tissue contact; (d) the force variation with the involuntary physiological motion; (e) images captured without passive linear structure; (f) images captured with passive linear structure.

lens tissue paper. To simulate the real surgical situation, we performed the hand-held scanning tests on freshly excised, acriflavine-stained porcine belly tissue. The experimental setup for hand-held experiments is shown in Fig. 8e. In the hand-held experiment, we performed the scanning five times. Due to large tissue deformation and hand moving, we failed two scans to get acceptable mosaicing results. We randomly chose two sets of dates from the left three trials for evaluation.

Figures 8f–8g show the examples of the mosaicings extracted from these experiments. Figure 8f illustrates a mosaicing that covers an area of approximately 10.79 mm^2. The ratio of the covered area to the intended area (15.73 mm^2) is 0.693. Figure 8g shows a second scan, where the mosaicing has an area of approximately 29.35 mm^2 (an area ratio of 0.72). It is

observed that the gaps between the spirals get larger than the mosaicing results of lens tissue paper during bench experiments. One reason for this was that the probe was not positioned vertically enough to the tissue during scanning. The other causes are likely to be the deformation of the specimen and hand moving during scanning. However, these images clearly demonstrated the key morphological features of porcine belly tissue. Most prominent were the adipocytes, and the large polygonal-shaped fat cells, while areas of fibrous tissue can also be clearly seen. In particular, the creation of the large area mosaicing enables global appreciation of the tissue characteristics.

The force variation during the hand-held experiments with porcine belly tissue is shown in Fig. 8h, which was mostly distributed between 0.07 and 0.60 N. The contact force was more undulate than that in
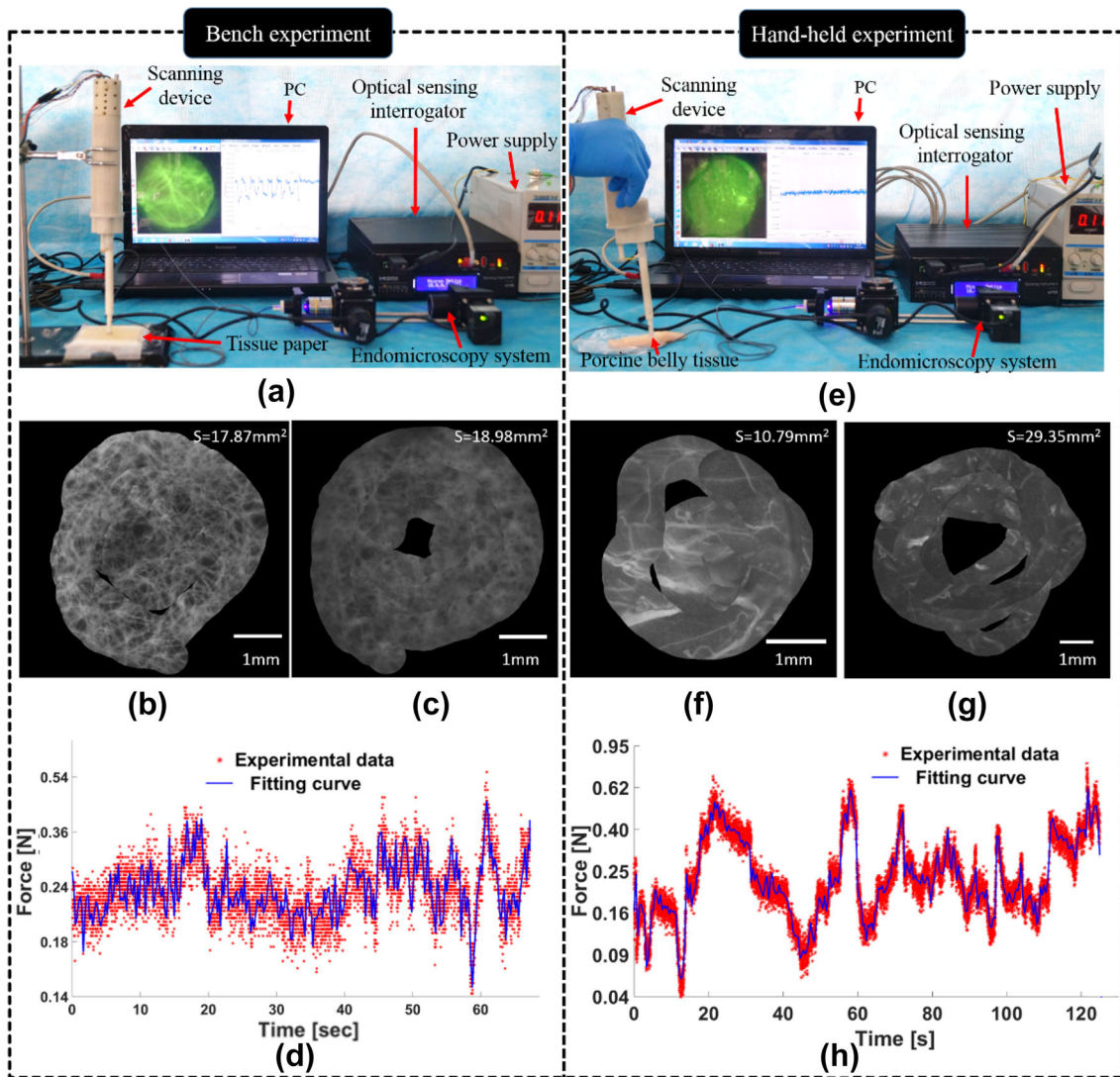
FIGURE 8. The mosaicing and force evaluation of the system, showing (a) the experiment setup for bench experiment with lens tissue paper; (b–c) the mosaicing results of lens tissue paper during bench experiments; (d) the force variation during the bench experiment with lens tissue paper; (e) the experiment setup for hand-held experiments with porcine belly tissue; (f–g) the mosaicing results of porcine belly tissue during hand-held experiments; (h) the force variation during the hand-held experiments with porcine belly tissue.

Fig. 8d, and sometimes was up to 1.12 N. The main reasons for this were deformation and the irregular surface of the porcine belly tissue.

DISCUSSION

In this paper, we have developed a robotic scanning device for confocal endomicroscopy, especially for application during the neck dissection or thyroidectomy. As a result, this device achieved large mosaicings up to 29.35 mm^2, which is a significant increase in area coverage compared to previous study. The actual size of the thyroid tumour was 0.79 cm in average.[18] The developed device can achieve a maximum 0.76 cm

diameter scanning surface, which verifies its feasibility of scanning tumour area. We expect that in clinical use, different tip units would be available to accommodate different sized tumours. A specially designed passive linear structure with force sensing was integrated into the device. Experimental results show that this structure is useful to compensate the hand tremor in axis direction as well as detect the contact force. During the hand tremor simulation tests, bench and hand-held experiments, a suitable range of contact force (0.07–0.60 N) for imaging acquisition[20,30] was consistently maintained. Although larger probe–tissue contact force can also obtain good quality imaging, it tends to drag the target tissue and make a large tissue deformation. Thus, it is not suitable to carry out a smooth

scanning motion. Generally, the passive structure in this study was an effective way to maintain good level probe–tissue contacts. The active linear actuation was used to ensure a suitable initial probe–tissue contact prior to each scanning instead of activation during the scanning, since the passive structure was sufficiently good for the clinical purpose of this study. For the flat tissue targets such as cavity created during thyroidectomy, passive structure may be enough for stable scanning. In case of large hollow and undulating surgical cavity, active feedback control of the linear structure would be important. Further work includes optimization of the passive linear structure design and the closed loop control of the active linear actuation from the FBG sensing feedback.

The contact or external forces usually affect the trajectory generated by an active actuation mechanism or move back and forth in actuation motion. However, the mechanical design in this study is an elegant passive actuation mechanism (limited by the spiral groove of the base frame). Hence, the trajectory of scanning tip is a constant and one way trip. Thus, this mechanical design could achieve accurate scanning trajectory even with tissue contact, demonstrated by the bench experiment. An undesired large tissue-probe contact force will reduce the travel distance and speed of the tip due to the deformation of the scanning shaft. Therefore, the area covered by scanning will be smaller than the designed value.

The FBG sensor is not easy to maintain and sensitive to the change of temperature. Since the FBG fiber has an ultra-low cost, it can be used as a disposable material requiring no maintenance. In this study, we tested the force sensing at a constant and stable room temperature. To realize a better sensitivity and accuracy of the FBG force sensing, temperature compensation methods and algorithms will be necessary. Various temperature compensation methods have been proposed.[22,38] For doing this, it may be necessary to include another FBG sensor or node.[21,32,37] However, this is not the focus of this paper.

We confirmed that the wavelength variation of the FBG sensor is mainly related to the probe–tissue contact force and has little relation with the type of contact material. Under the same contact force, although the deformation of the materials are different, the compression status of FBG sensor should be the same, which results in the same wavelength variation of FBG sensor. One limitation is that the probe needs to be positioned vertically to the tissue during scanning to achieve targeted mosaicing. Axial force is the key to obtaining good quality imaging. Thus, we designed the FBG sensor unit that can only be compressed along the axial direction to sense axial force and can't be deformed in the transverse direction.

It is important to achieve speedy and effective scanning. The maximum tangential velocity of the probe that could obtain consistent mosaicing was 1.91 mm/s in this study. It took almost 66 s to reach the targeted scanning area of 29.35 mm^2 as shown in Fig. 8g. Currently, the waiting time of frozen section to examine tumour margins is approximately 40 min, and specimen X-rays will take 5–10 min but it has low accuracy rates. Thus, the ability of the device to obtain large area cellular imaging with about a minute is effective for surveillance of residual tumour distribution in the target area. An unreasonable high linear velocity of scanning tip would ruin a scan. It is necessary to ensure sufficient overlap between image frames for robust mosaicing. The frame rate of the endomicroscopy system is 15 Hz in this study. We found experimentally that a shift of 136 μm between images (an overlap of 664 μm) was necessary to ensure consistent results, implying a maximum acceptable linear velocity of 1.91 mm/s. It will fail the mosaicing if the linear velocity is more than 1.91 mm/ s. In the case of using the device as hand-held instrument, motion artefacts including large hand moving, breathing or other patient motion that could affect the proper probe–tissue contacts may also ruin a scan.

The base frame with spiral groove was specially designed and fabricated by wire-cut EDM. This manufacturing method achieves high precision for the spiral groove, thus allowing smaller hysteresis error and higher repeatability. In this study, we have presented detailed results of trajectory evaluation using an NDI Aurora EM tracking system. The results indicate that the probe can cover a large spiral trajectory. We observed errors in the results from theoretical value. The main cause of the deviation is likely to be the combination of the gap tolerance errors between the Nitinol lever and spiral groove, elastic deformation of the Nitinol lever, the vibration of the shaft during scanning and the noise by EM tracking system itself. As the field-of-view captured by the endomicroscopy system is 0.8 mm in diameter and the spiral loop spacing of the scanning trajectory is designed to be 0.8 mm, the positioning errors at the tip may result in gaps between the loops of spiral mosaicing. The mosaicing results of lens tissue paper (Figs. 8b and 8c) show good quality images with small gaps. These mosaicing results demonstrate that the actual trajectories of the tip could follow the target positions at an acceptable level.

In bench experiments with lens tissue paper, the results demonstrate that the device can scan the tissue stably, and the motion of the probe and the image quality are suitable for generating large area mosaicing. We also show that the probe can maintain a

consistent contact over large area of porcine tissue during the hand-held experiment. However, gaps in mosaicing were observed due to the deformation and irregularity surface of porcine belly tissue, and the random hand tremor in horizontal directions. Nevertheless, this still allows visualisation of a large area and should be satisfactory for diagnosis purpose.

During the scanning, the device can be fixed on an arm or hand-held by the doctor. The size and weight of the device is suitable for easy manoeuvrability. The compactness and simplicity of the design also increase the feasibility of commercialization in the future. The tip modules of the device can be separated easily, thus it is suitable for using in a patient-specific design process such as being equipped with different endomicroscopy probes, sensing units, scanning trajectories and lengths of scanning shaft. In future, by using visual servoing to correct the scanning trajectory, it is possible to further enhance the current mosaicing algorithm. Overall, this robotic scanning device is a robust and economical platform to generate consistent images in real-time to help making intraoperative decisions.

CONCLUSION

In this paper, we have demonstrated and characterised a new robotic scanning device that can cover a large field-of-view in confocal endomicroscopy during the neck dissection or thyroidectomy. The device can scan a large surface in a spiral trajectory by rotating the tip frame along the spiral groove of the base frame. Probe–tissue contact force can be detected by the FBG sensor during the scanning. Furthermore, the passive linear structure is useful to compensate hand tremor and provide a stable contact between probe and tissue. We have demonstrated the possibility of scanning over large surfaces using lens tissue paper and *ex vivo* porcine belly tissue. The mosaicing and force sensing results show that the scanning device allows high quality imaging with consistent probe–tissue contact over a large surface area. The results demonstrate the potential clinical value of the device to improve the prospects for intraoperative tumour margin evaluation.

CONFLICT OF INTEREST

None.

REFERENCES

[1]Ayache, N., T. Vercauteren, G. Malandain, F. Oberrietter, N. Savoire, and A. Perchant. Processing and mosaicing of fibered confocal images. In: MICCAI Workshop on Microscopic Image Analysis with Applications in Biology (MIAAB'06), 2006.

[2]Balicki, M., A. Uneri, I. Iordachita, J. Handa, P. Gehlbach, and R. Taylor. Micro-force sensing in robot assisted membrane peeling for vitreoretinal surgery. *Med. Image Comput. Comput. Assist. Interv.* 13:303–310, 2010.

[3]Becker, V., T. Vercauteren, C. H. von Weyhern, C. Prinz, R. M. Schmid, and A. Meining. High-resolution probe-based confocal microscopy in combination with video mosaicing (with video). *Gastrointest. Endosc.* 66(5):1001–1007, 2007.

[4]Bedard, N., T. Quang, K. Schmeler, R. Richards-Kortum, and T. S. Tkaczyk. Real-time video mosaicing with a high-resolution microendoscope. *Biomed. Opt. Express.* 3(10):2428–2435, 2012.

[5]Chandra, S., E. C. Gorospe, C. L. Leggett, and K. K. Wang. Barrett's esophagus in 2012: updates in pathogenesis, treatment, and surveillance. *Curr. Gastroenterol. Rep.* 15(5):1–6, 2013.

[6]Chang, T. P., F. Palazzo, N. Tolley, V. Constantinides, G. Z. Yang, and A. Darzi. Vascularity assessment of parathyroid glands using confocal endomicroscopy: towards an intraoperative imaging tool for real-time *in situ* viability assessment. *Eur. J. Surg. Oncol.* 40(12):1799, 2014.

[7]Chang, T. P., K. Sriskandarajah, T. P. Cundy, D. R. Leff, R. C. Newton, H. J. Marcus, A. Darzi, and G. Z. Yang. Anatomical neck dissection for real time intraoperative *in vivo in situ* soft tissue morphology characterization using confocal endomicroscopy. In: The Hamlyn Symposiμm on Medical Robotics, 94 pp., 2013.

[8]Choi, D. Y., and C. N. Riviere. Flexure-based manipulator for active handheld microsurgical instrument. In: 27th Annual International Conference of the Engineering in Medicine and Biology Society, IEEE-EMBS 2005, pp. 2325–2328. IEEE.

[9]Dwyer, G., P. Giataganas, P. Pratt, M. Hughes, and G. Z. Yang. A miniaturised robotic probe for real-time intraoperative fusion of ultrasound and endomicroscopy. In: Proceedings of IROS, pp. 1196–1201, 2015.

[10]Enomoto, K., S. Uchino, H. Noguchi, Y. Enomoto, and S. Noguchi. A novel surgical technique for thyroid cancer with intra-cricotracheal invasion: windmill resection and tetris reconstruction. *Indian J. Surg.* 77(2):319–326, 2015.

[11]Erden, M. S., B. Rosa, N. Boularot, B. Gayet, G. Morel, and J. Szewczyk. Conic-Spiraleur: a miniature distal scanner for confocal microlaparoscope. *IEEE/ASME Trans. Mechatron.* 19(6):1786–1798, 2014.

[12]Erden, M. S., B. Rosa, N. Boularot, B. Gayey, and G. Morel. Conic-Spiraleur: a miniature distal scanner for confocal microlaparoscope. *IEEE/ASME Trans. Mechatron*. 19(6):1786–1798, 2014.

[13]Gonenc, B., M. A. Balicki, J. Handa, P. Gehabach, C, N. Riviere, R. H. Tylor, and I. Iordachita. Evaluation of a micro-force sensing handheld robot for vitreoretinal surgery. In: Proceedings of IROS, pp. 4125–4130, 2012.

[14]Guo, Y., J. Kong, H. Liu, H. Xiong, G. Li, and L. Qin. A three-axis force fingertip sensor based on fiber Bragg grating. *Sens. Actuators A. Phys*. 249:141–148, 2016.

[15]He, X., J. Handa, P. Gehlbach, R. Taylor, and I. Iordachita. A submillimetric 3-DOF force sensing instrument with integrated fiber Bragg grating for retinal microsurgery. *IEEE Trans. Biomed. Eng*. 61(2):522–534, 2014.

[16]Hill, K. O., and G. Meltz. fiber Bragg grating technology fundamentals and overview. *J. Lightw. Technol*. 15(8):1263–1276, 1997.

[17]Jabbour, J. M., M. A. Saldua, J. N. Bixler, and K. C. Maitland. Confocal endomicroscopy: instrumentation and medical applications. *Ann. Biomed. Eng*. 40(2):378–397, 2012.

[18]Kang, S. W., J. J. Jeong, J. S. Yun, T. Y. Sung, S. C. Lee, Y. S. Lee, et al. Robot-assisted endoscopic surgery for thyroid cancer: experience with the first 100 patients. *Surg. Endosc*. 23(11):2399, 2009.

[19]Kreike, B., A. A. M. Hart, T. V. D. Velde, J. Borger, H. Peterse, E. Rutgers, H. Bartelink, and M. J. van de Vijver. Continuing risk of ipsilateral breast relapse after breast-Novel Balloon Surface Scanning Deviceconserving therapy at long-term follow-up. *Int. J Radiat. Oncol. Biol. Phys*. 71(4):1014–1021, 2008.

[20]Latt, W. T., R. C. Newton, M. Visentini-Scarzanella, C. J. Payne, D. P. Noonan, J. Shang, and G. Z. Yang. A handheld instrument to maintain steady tissue contact during probe-based confocal laser endomicroscopy. *IEEE Trans. Biomed. Eng*. 58(9):2694–2703, 2011.

[21]Li, T., Y. Tan, Z. Zhou, and K. Zheng. A non-contact FBG vibration sensor with double differential temperature compensation. *Opt. Rev*. 23(1):26–32, 2016.

[22]Magne, S., S. Rougeault, M. Vilela, and P. Ferdinand. State-of-strain evaluation with fiber Bragg grating rosettes: application to discrimination between strain and temperature effects in fiber sensors. *Appl. Opt*. 36(36):9437–9447, 1997.

[23]Mahé, J., T. Vercauteren, B. Rosa, and J. Dauguet. A viterbi approach to topology inference for large scale endomicroscopy video mosaicing. *Proc. MICCAI* 16:404–411, 2013.

[24]Mark, P., D. Yu, and R. K. Rebecca. High-resolution fiber-optic micro endoscopy for *in situ* cellular imaging. *J. Vis. Exp*. 47(47):e2306–e2306, 2011.

[25]Meining, A., M. Bajbouj, S. Delius, and C. Prinz. Confocal laser scanning microscopy for *in vivo* histopathology of the gastrointestinal tract. *Arab. J. Gastroenterol*. 8(1):1–4, 2007.

[26]Newton, R. C., S. V. Kemp, P. Shah, D. Elson, A. Darzi, K. Shibuya, S. Mulgrew, and G. Z. Yang. Progress towardoptical biopsy: bringing the microscope to the patient. *Lung* 189(2):111–119, 2011.

[27]Newton, R. C., S. V. Kemp, G. Z. Yang, A. Darzi, M. N. Sheppard, and P. L. Shah. Tracheobronchial amyloidosis and confocal endomicroscopy. *Respiration* 82(2):209–211, 2011.

[28]Newton, R. C., S. V. Kemp, G. Z. Yang, D. Ellson, A. Darzi, and P. Shah. Imaging parenchymal lung diseases with confocal endomicroscopy. *Respir. Med*. 106(1):127–137, 2012.

[29]Newton, R. C., S. V. Kemp, G. Z. Yang, D. S. Elson, A. Darzi, and P. L. Shan. Imaging parenchymal lung diseases with confocal endomicroscopy. *Respir. Med*. 106(1):127–137, 2012.

[30]Newton, R. C., D. Noonan, C. Payne, J. Andreyev, A. Di Marco, M. V. Scarzanella, A. Dari, and G. Z. Yang. Probe tip contact force and bowel distension affect crypt morphology during confocal endomicroscopy. *Gut* 60:A12–A13, 2011.

[31]Noonan, D. P., D. S. Elson, G. P. Mylonas, A. Darzi, and G. Z. Yang. Laser-induced fluorescence and reflected white light imaging for robot-assisted MIS. *IEEE. Trans. Biomed. Eng*. 56(3):889–892, 2009.

[32]Park, Y. L., S. C. Ryu, R. J. Black, K. Chau, B. Moslehi, and M. R. Cutkosky. Exoskeletal force-sensing end-effectors with embedded optical fiber-Bragg-grating sensors. *IEEE. Trans. Robot*. 25(6):1319–1331, 2009.

[33]Rosa, B., B. Herman, J. Szewczyk, B. Gayet, and G. Morel. Laparoscopic optical biopsies: *in vivo* robotized mosaicing with probe-based confocal endomicroscopy. In: Proceedings of IROS, pp. 1339–1345, 2011.

[34]Russo, S., P. Dario, and A. Menciassi. A novel robotic platform for laser assisted transurethral surgery of the prostate. *IEEE Trans. Biomed. Eng*. 62(2):489–500, 2015.

[35]Singletary, S. E. Surgical margins in patients with early-stage breast cancer treated with breast conservation therapy. *AM. J. Surg*. 184(5):383–393, 2002.

[36]Vercauteren, T., A. Perchant, G. Malandain, X. Pennec, and N. Ayache. Robust mosaicing with correction of motion distortions and tissue deformations for *in vivo*, fibered microscopy. *Med Image Anal*. 10(5):673–692, 2006.

[37]Wei, J., S. Wang, J. Li, and S. Zuo. Novel integrated helical design of single optic fiber for shape sensing of flexible robot. *IEEE. Sens. J*. 2017. https://doi.org/10.1109/JSEN.2017.2748162.

[38]Xu, M. G., J. L. Archambault, L. Reekie, and J. P. Dakin. Discrimination between strain and temperature effects using dual-wavelength fibre grating sensors. *Electron. Lett*. 30(13):1085–1087, 1994.

[39]Yeh, M. W., A. J. Bauer, V. A. Bernet, R. L. Ferris, L. A. Loevner, S. J. Mandel, L. A. Orloff, G. W. Randolph, and D. L. Steward. American Thyroid Association statement on preoperative imaging for thyroid cancer surgery. *Thyroid* 25(5):3–14, 2015.

[40]Zuo, S., M. Hughes, and G. Z. Yang. Novel balloon surface scanning device for intraoperative breast endomicroscopy. *Ann. Biomed. Eng*. 44(7):2313–2326, 2015.

[41]Zuo, S., M. Hughes, and G. Z. Yang. Flexible robotic scanning device for intraoperative endomicroscopy in MIS. In: IEEE/ASME Transactions on Mechatronics, 99 pp., 2017.

[42]Zuo, S., M. Hughes, P. Giataganas, and C. Seneci. Development of a large area scanner for intraoperative breast endomicroscopy. In: Proceedings of IROS, pp. 3524–3530, 2014.

[43]Zuo, S., and G. Z. Yang. Endomicroscopy for computer and robot assisted intervention. *IEEE. Rev. Biomed. Eng*. 2017. https://doi.org/10.1109/RBME.2017.2686483.